









Artificial Intelligence and Numerical Methods Aided Design of Patient-Specific Coronary Stents

William Solórzano-Requejo^{1,2}^a, Carlos Aguilar¹^b, Rodrigo Zapata Martínez¹^c, Oscar Contreras-Almengor³^d, Isabel Moscol²^e, Carlos Ojeda²^f, Jon Molina-Aldareguia^{1,3}^g and Andrés Díaz Lantada¹^h

¹ETSI Industriales, Universidad Politécnica de Madrid, Madrid, Spain

²Department of Mechanical and Electrical Engineering, Universidad de Piura, Piura, Peru

³IMDEA Materials Institute, Getafe, Spain

Keywords: Machine Learning, Computational Design, Personalized Medicine, Automated Design, Additive Manufacturing.


Abstract: The design of personalized medical devices, which are adapted to the patient's needs, starts from a digital model created from the advanced use of clinical imaging techniques such as magnetic resonance imaging or computed tomography. However, this methodology has several sources of error related to the medical imaging acquisition, segmentation and reverse engineering process, tessellation, and the selected additive manufacturing technique. Therefore, this paper proposes a new design strategy that avoids medical image segmentation. To demonstrate its feasibility, a patient-specific coronary stent was designed and manufactured based on slices similar to medical images. Using artificial intelligence algorithms and numerical methods, the ellipse that best fit the patient's artery was obtained, and finally customized stent was generated from the parameterization of unit cells, demonstrating that it is possible to semi-automate the design of biodevices by removing some sources of error inherent to the conventional workflow.


1 INTRODUCTION


Cardiovascular diseases have become an increasingly serious threat to human life. In particular, coronary artery disease is a major health and economic burden, and the third leading cause of death worldwide (Scafa Udriște et al., 2021). It develops when fatty substances, such as fat, calcium, and cellular debris, are deposited in the arterial wall obstructing blood flow and triggering an inadequate supply of oxygen and nutrients to the myocardium, potentially inducing a heart attack, brain haemorrhage or ischemic stroke (Pan et al., 2021).


The most common treatment is the percutaneous coronary intervention (PCI), a minimally invasive and effective surgery used to clean the artery by introducing a tubular metallic structure (stent) inside it, whose objective is to restore the cardiovascular system function through the expansion of the arterial wall, decreasing the risk of restenosis (Saçlı et al., 2018).


Top-class coronary stent must have mechanical properties like high elasticity and flexibility to allow coiling and expansion in the blood vessel; high radial and fatigue strength to withstand periodic physiological loads; good biocompatibility to reduce the incidence of thrombosis and restenosis and good


^a  <https://orcid.org/0000-0002-2989-9166>


^b  <https://orcid.org/0000-0003-0291-3041>


^c  <https://orcid.org/0000-0002-2611-7050>

^d  <https://orcid.org/0000-0002-8166-4161>

^e  <https://orcid.org/0000-0001-8959-9547>

^f  <https://orcid.org/0000-0001-6163-5382>

^g  <https://orcid.org/0000-0003-3508-6003>

^h  <https://orcid.org/0000-0002-0358-9186>

radiopacity on fluoroscopy for long-term follow-up (Cockerill et al., 2021; Scafa Udriște et al., 2021; Tomberli et al., 2018). Stents are prevalently manufactured with standard dimensions and shapes. Surgeons select the one that best fits the patient’s anatomy. However, mismatch between the implant and the anatomy affects its performance and lifespan.

Follow-up studies have proven that, one year after implantation, the probability of restenosis is up to 40%, and around 10% of patients need a new prosthesis (Pan et al., 2021; Schillinger et al., 2007). This is the consequence of geometrical changes in a coronary artery after surgery due to the difference in size between the expanded stent and the blood vessel. If the stent does not fit to the diseased artery, a strong interaction force will be generated resulting in stress concentration, damaging the artery, and eventually leading to restenosis (Wang et al., 2018). This pathology is a major challenge; therefore, the combination of medical and mechanical design can improve significantly the function of vascular prostheses to meet the needs of patients and hospitals worldwide.

Current trends around the production and design of personalized medical devices have integrated clinical information about the patient’s anatomy, ranging from single-unit production using manual techniques to fully automated manufacturing with a rapid, non-invasive and more accurate approach (Paxton et al., 2022).

Soft tissue reconstruction from computed tomography (CT) or magnetic resonance (MR) slices provides an additional view of the patient’s pathological state that helps to optimize stent fitting.

This whole process, including the reconstruction, personalized design, and manufacturing to get the final cardiovascular device entails a high computational cost and has several sources of error (Díaz Lantada et al., 2022).

Around the slice acquisition, as consequence of the resolution (pixels) and the thickness of the slices, an error occurs because to reconstruct the 3D model the designer must properly select the voxels that compose it (segmentation). Then, it will be exported as an STL file, which gives rise to the second error resulting from the separation between voxels and triangular facets due to the action of smoothing tools. This digital artery allows the designer to model the custom medical device and export it as an STL file, generating the third error due to the tessellation process (Figure 1).

Custom-made implants are generally produced with additive manufacturing (AM) technology. Depending on the type of AM, different layer heights are required, creating a staircase effect. The error associated with this effect is less significant compared to the medical imaging acquisition, due to the differences in the magnitudes of the layer thickness, however, this generates the fourth source of error (Figure 1).

All the errors described affect the final product. Although the inaccuracy associated with medical image and the selected manufacturing process is not easy to avoid, the one related to segmentation can be mitigated by capturing the patient’s physiologic information from the image, using an algorithm that extracts its edge and allows the designer to model on it. This is the objective of this paper, focused on

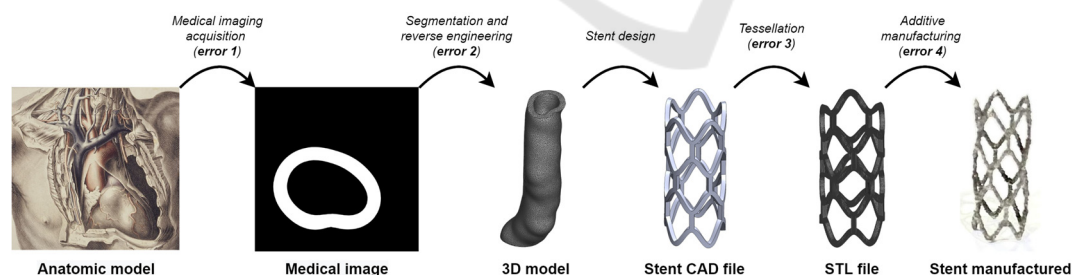


Figure 1: Patient-specific stent workflow errors.

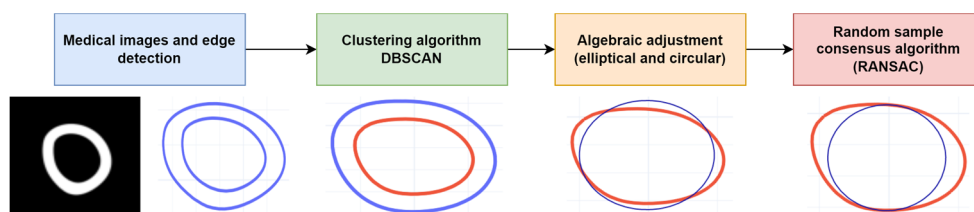


Figure 2: Roadmap.

coronary stents, which integrates artificial intelligence, numerical methods, and computer-aided design to produce personalized implants that reduce the possibility of failure.

2 MATERIALS AND METHODS

This section details the basics of medical image edge extraction (2.1), inner and outer edge separation (2.2), algebraic fitting (2.3), and enhancement employing the random sample consensus algorithm (RANSAC, 2.4) to obtain information from tomographic slices of a coronary artery and design a stent that matches the patient's anatomy (Figure 2).

2.1 Medical Images and Edge Detection

This study, as a proof of concept, does not intend to focus on CT or MR image processing due to its high complexity. Therefore, Chitubox[®]v1.9.0 (Chitubox, Zhongcheng Future Industrial Park, Hangcheng Avenue, Baoan District, Shenzhen, Guangdong, China 518128), an open-source program for manufacturing 3D models with digital light processing (DLP) technology, was used to obtain axial tomographic images, properly setting parameters such as number of pixels (resolution), printing table dimensions and layer height. When the STL file is imported into the software, black-and-white images are generated from bottom to top, going through the file layer by layer, producing medical-like slices which in this research will be considered as medical images (Moscol et al., 2022).

Edge detection plays an important role in determining the inner radius of the artery and adapting the stent to it. One method to recognize the edge consists of identifying pixels with different intensities; however, the result was not adequately adjusted (Figure 3). Therefore, a new edge detector, based on the partial area effect that does not assume continuity in pixel intensity values, was used to achieve highly accurate extraction of edge position, orientation and curvature in challenging conditions such as images with noise, blurred edges, low contrast areas or very close edges (Trujillo-Pino et al., 2013).

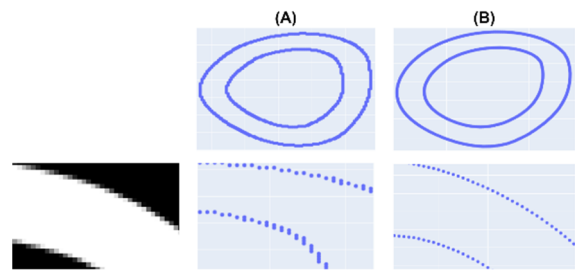


Figure 3: Edge detection at the (A) pixel and (B) subpixel level.

To use this algorithm (Trujillo-Pino et al., 2013), the medical images, a 3D matrix whose rows and columns correspond to the number of pixels, were converted to grayscale to get a 2D array whose pixel intensities range from 0 to 255. In addition, three hyperparameters were defined: the threshold, which allows the algorithm to distinguish an edge if the difference in intensities in two adjacent regions exceeds 120; a zero-order filter, to detect the edge without noise; and the order of the edge to be adjusted (second order).

2.2 Clustering Algorithm

The coordinates of the points extracted from the edge are represented in the pixel domain, but they must be converted into millimetres for the biodevice design. For this, the origin is defined in the centre of the image and an equivalence is made between the resolution and printing table dimensions configured in Chitubox[®].

The image is composed of two edges: internal and external. However, the information required by the designer is provided by the inner part, and to separate them automatically the density-based spatial clustering of application with noise (DBSCAN) algorithm was used.

The main idea of this technique is that two points are considered neighbours if the distance between them is less than or equal to “*eps*” and the minimum number of points to define a cluster is “*min_sample*”. Hence, it is implemented by setting both hyperparameters for the images, the values of *min_samples* and *eps* were determined as 3 and 0.7 respectively.

2.3 Algebraic Fitting

2.3.1 Elliptical

The points of the inner edge, acquired with the DBSCAN algorithm, allow a curve to be fitted for

automatically taking the measurement of the artery and adjust the design to them. The ellipses, in particular, adapt to the shapes and sizes of complex anatomical sections (Solórzano-Requejo et al., 2022), so the basic principles of their algebraic fitting are detailed. The fitted ellipse is represented by an implicit second-order polynomial (Q), defined by a vector of coefficients ($v = [A B C D E F]^T$):

$$Q(p, v) = [x^2 \quad xy \quad y^2 \quad x \quad y \quad 1] \cdot \begin{bmatrix} A \\ B \\ C \\ D \\ E \\ F \end{bmatrix} = 0 \quad (1)$$

If $P = \{p_1, p_2, \dots, p_n\}$ is the set of points of the inner edge, the vector of coefficients must be adjusted to it, so the algebraic distance (D_A) is used because it simplifies the calculations and requires less computational resources (Fitzgibbon et al., 1999). Mathematically, it is obtained by substituting the coordinates of a point $p_i = (x_i, y_i)$ in the polynomial Q , therefore, if p_i belongs to the ellipse its distance will be zero:

$$D_A(p_i, v) = Ax_i^2 + Bx_iy_i + Cy_i^2 + Dx_i + Ey_i + F \quad (2)$$

The least-squares technique optimized the fit by minimizing the square of the algebraic distance between P and the adjusted ellipse Q , which can be expressed as the squared norm of the product between the design matrix D_P , which contains information of P , and v .

$$D_P = \begin{bmatrix} x_1^2 & x_1 & y_1 & y_1^2 & x_1 & y_1 & 1 \\ x_2^2 & x_2 & y_2 & y_2^2 & x_2 & y_2 & 1 \\ \vdots & \vdots & \vdots & \vdots & \vdots & \vdots & \vdots \\ x_n^2 & x_n & y_n & y_n^2 & x_n & y_n & 1 \end{bmatrix} \quad (3)$$

$$\min \sum_{i=1}^n D_A(p_i, v)^2 = \min \|D_P v\|^2 \quad (4)$$

To avoid the trivial solution of $v = \bar{0}_6$, v is bounded with a constraint of $\|v\|^2 = 1$, preventing that all coefficients are zero (Paton, 1970). Lagrange multipliers allow to minimize the distance considering this condition:

$$L = v^T D_P^T D_P v - \lambda(v^T v - 1) \quad (5)$$

To minimize L , its gradient with respect to v is set to 0:

$$\nabla_v L = 0 \Leftrightarrow 2D_P^T D_P v - 2\lambda v = 0 \quad (6)$$

$$D_P^T D_P v = \lambda v \quad (7)$$

Equation (7) leads to the eigenvector problem, then λ and v must be an eigenvalue and eigenvector of $D_P^T D_P$. If $D_P^T D_P v = \lambda v$, equation (4) will be:

$$\min v^T D_P^T D_P v = \min \lambda \|v\|^2 = \min \lambda \quad (8)$$

Consequently, the coefficient vector (v) that minimizes the distance will be the eigenvector of $D_P^T D_P$ corresponding to the smallest eigenvalue (λ).

2.3.2 Circular

For cardiovascular prosthesis, it may be more interesting to fit a circle to the inner wall of blood vessels. Therefore, this subsection describes the theory related to its algebraic fitting (Černov, 2011). Starting from the general equation of the circle (f) and developing it:

$$f = [x^2 \quad xy \quad y^2 \quad x \quad y \quad 1] \cdot \begin{bmatrix} 1 \\ 0 \\ 1 \\ -2k \\ -2m \\ k^2 + m^2 - r^2 \end{bmatrix} = 0 \quad (9)$$

Linking equation (1) to (9), it is determined that $A = C = 1$, $B = 0$, $D = -2k$, $E = -2m$ and $F = k^2 + m^2 - r^2$. Therefore, D_A from a point $p_i = (x_i, y_i)$ to the fitted circle is:

$$D_A(D, E, F, p_i) = x_i^2 + y_i^2 + D \cdot x_i + E \cdot y_i + F \quad (10)$$

To find the values of D , E and F defining the fitted curve, the algebraic distance squared of the “ n ” points composing the inner edge is minimized:

$$D_A^2 = \min \sum_{i=1}^n (x_i^2 + y_i^2 + D \cdot x_i + E \cdot y_i + F)^2 \quad (11)$$

For this purpose, D_A^2 is partially derived with respect to D , E and F , equating to 0 and rewritten in matrix form:

$$\begin{bmatrix} \sum x_i^2 & \sum x_i \cdot y_i & \sum x_i \\ \sum x_i \cdot y_i & \sum y_i^2 & \sum y_i \\ \sum x_i & \sum y_i & n \end{bmatrix} \cdot \begin{bmatrix} D \\ E \\ F \end{bmatrix} = \begin{bmatrix} \sum -(x_i^2 + y_i^2) \cdot x_i \\ \sum -(x_i^2 + y_i^2) \cdot y_i \\ \sum -(x_i^2 + y_i^2) \end{bmatrix} \quad (12)$$

Solving the linear system, the coefficients of the fitted circumference are obtained.

2.4 RANSAC Algorithm

The random sample consensus algorithm (RANSAC), published by Fischler and Bolles

(Fischler & Bolles, 1981), is an iterative method for estimating the parameters of a mathematical model from a dataset containing outliers. RANSAC proposes to create a cost function that sums the distance of the points to the fitted curve and iteratively select some of them to fit again and choose the one that produces the lowest cost.

Due to the iterative nature of the algorithm, it is not deterministic, and the model obtained may not be the best. Nevertheless, it is a useful tool to integrate with the elliptical and circular fitting, presented in the previous sections, since in personalized implant design it is required that the fitted curve adapts as well as possible to the inner edge without exceeding it. If

only the algebraic fitting is used, the result does not meet this condition, so it is necessary to integrate this procedure to RANSAC (Figure 2).

Compared to the algebraic fitting that squares the distance to make the function convex and ensure that a minimum exists, the modified RANSAC algorithm takes advantage of the sign of the algebraic distance (cost function) to determine whether the adjusted curve is inside or outside the edge. This innovative approach is interesting and can be applied to image processing and computer vision tasks.

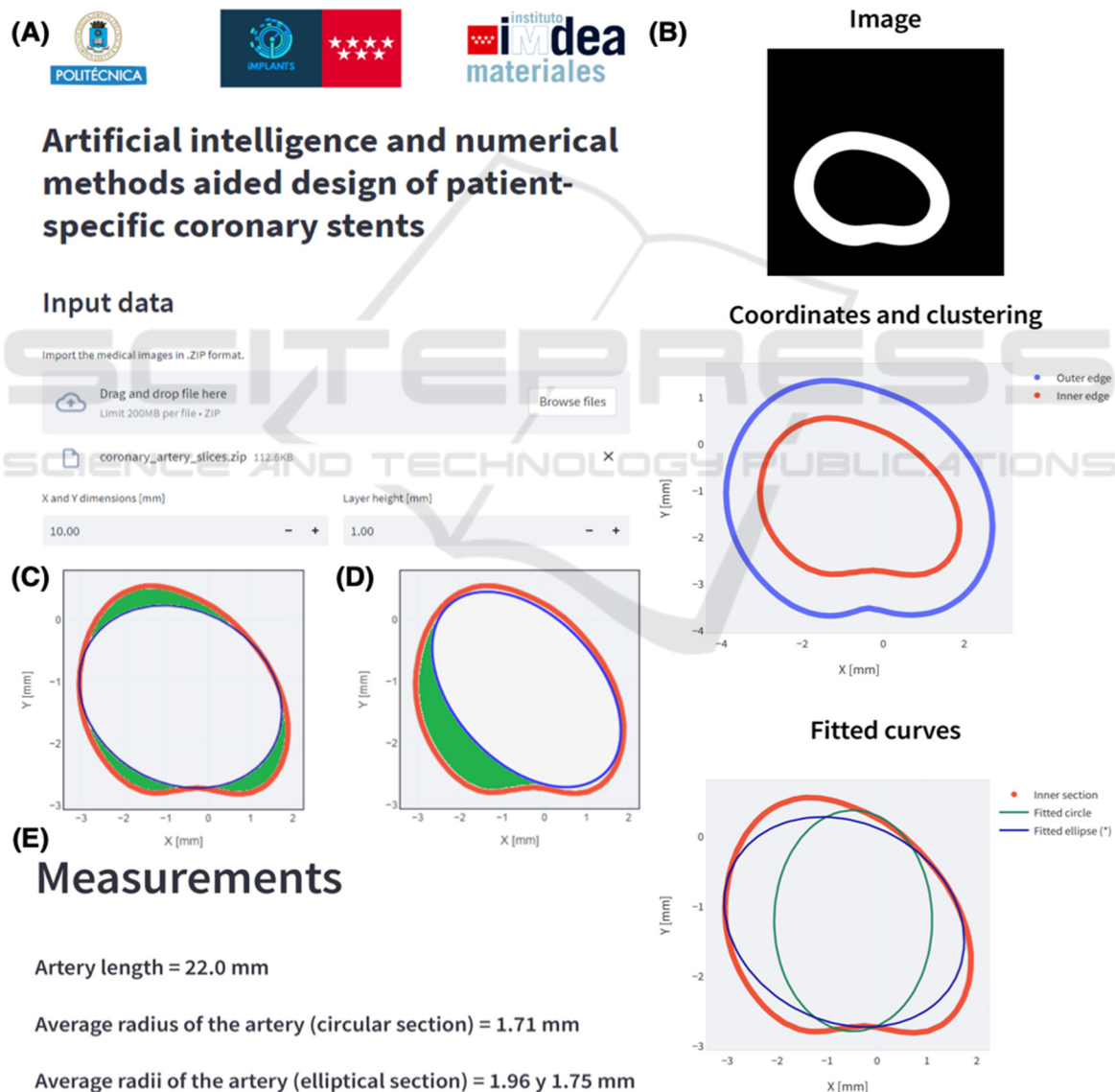


Figure 4: (A) Web application. (B) Coronary artery slice fits. Comparison between (C) the fit provided by the application and (D) another possible solution. (E) Output of the web application.

3 RESULTS AND DISCUSSION

3.1 Web Application and Virtual Model

In order to integrate the explained algorithms and to encourage the symbiotic use of computer aided design, artificial intelligence and numerical methods in the design of personalized biodevices, a web app has been developed with the Streamlit library (*Streamlit*, n.d.) of Python® 3.7.14 (Phyton Software Foundation) as it allows the deployment of apps in a simple way.

As mentioned above, two different approaches were used to assist the parametric design of personalized coronary stents. The circular algebraic fitting which, in most cases, does not appropriately adjust the patient's coronary topology and a new innovative and more suitable approach, the elliptical one.

To prove the effectiveness of both methods, a virtual STL model of a patient's artery has been used. The STL file (Model ID 3DPX-012589), based on a CT scan and segmented by researchers at the University of Toronto and Toronto General Hospital, has been downloaded from the NIH 3D Print Exchange repository (*Phantom Coronary Artery Models | NIH 3D Print Exchange*, n.d.) and imported into Chitubox® by setting up the resolution, print plate dimensions and layer height as 512×512 pixels, $10 \times 10 \times 22$ mm and 1 mm respectively. Finally, the 3D model was sliced, and each image has been stored in a general .ZIP file.

The .ZIP archive has been uploaded in the web application (Figure 4A) by introducing the parameters configured in Chitubox® to transform pixel into coordinates and compute the algebraic distance, used as cost function to get the circle or ellipse that best fits the arterial wall to cause minimal long-term restenosis (Figure 4C & D). The app outputs, for each slice, the circular and elliptical algebraic fitting (Figure 4B), the average radius or radii and length of the artery, parameters that will be introduced into the parametric design (Figure 4E).

3.2 Parametric Design of Coronary Stents

The stent designs are based on a geometry unit cell (Figure 5C) that is repeated bidirectionally, resulting in a 2D mesh (Figure 5D) that folds back on itself to form the stent (Figure 5E) and then deforms to obtain the elliptical cross-section (Figure 5F). The modelling

of these unit cells is parameterised according to the web app outputs, the average radius (R) and length (L), in addition, for the elliptical adjustment, the major (R_1) and the minor average radius (R_2). The number of unit cell repetitions (N_x and N_y) in the transversal (X) and radial (Y) axes, and the thickness (t) can be modified as the designer requires.

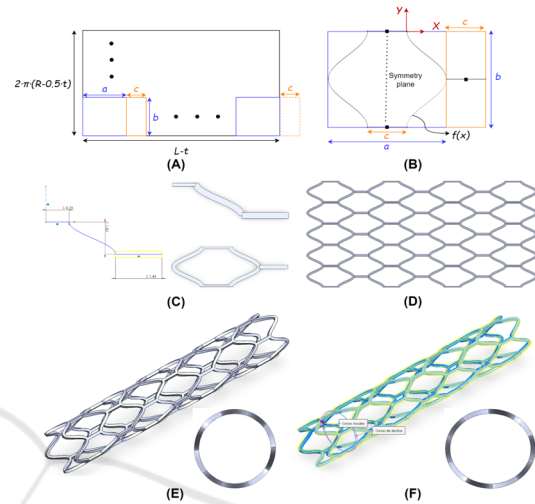


Figure 5: (A) Macroscopic and (B) microscopic view of coronary stent model. (C) Unit cell and (D) mesh construction. (E) Circular and (F) elliptical parametrized stent.

As an example, the entire parametrized design workflow can be seen in Figure 5. Macroscopically, the unit cell, in most cases, is a $a \times b$ rectangle that will repeat N_x and N_y times in the X and Y axis, respectively. When figuring a and b measures, the thickness of the stent must be considered. In this example, unit cells connectors must be also taken into consideration, resulting in a $(a + c) \times b$ rectangle. Therefore, the width of the mesh will be $2 \times \pi \times (R - 0.5 \cdot t)$ and the dimension of b :

$$b = \frac{2\pi(R - 0.5t)}{N_y} \quad (13)$$

The relation between the mesh and unit cell length is (Figure 5A):

$$L - t = N_x(a + c) - c \quad (14)$$

Microscopically, the unit cell has a specific shape bounded by the $a \times b$ rectangle, hence, the mathematical relation between macroscopic and microscopic parameters must be established. To simplify the parametrization, the length of the unit cell (a) and the connector length (c) was set as follows (Figure 5B):

$$c = \frac{a}{3} \quad (15)$$

Introducing (15) into (14), the value of a is defined as a function of L , N_x and t :

$$a = \frac{L - t}{\frac{4}{3}N_x - \frac{1}{3}} \quad (16)$$

The curve $f(x)$ used in the unit cell follows the sinusoidal equation parametrized as a function of b and c . Where $\frac{c}{2}$ is the amplitude and the vertical offset, $\frac{2\pi}{b}$ the period and $\frac{b}{4}$ the phase shift (Figure 5B).

$$f(x) = \frac{c}{2} \cdot \sin\left(\left(\frac{2\pi}{b}\right)\left(x - \frac{b}{4}\right)\right) + \frac{c}{2}; \quad (17)$$

$$x \in [0, 0.5b]$$

This geometry has been designed and parametrized in Solidworks® 2021 (Dassault Systèmes SolidWorks Corporation, UK). To validate its suitability, the web outputs has been introduced in the parametric file described above where N_x , N_y and t has been set as 4, 5 and 0.2 mm respectively. Then, the patient-specific stent has been exported in STL format to manufacture prototypes using AM techniques such as stereolithography (Figure 6B), selective laser sintering (Figure 6C) and selective laser melting (Figure 6D).

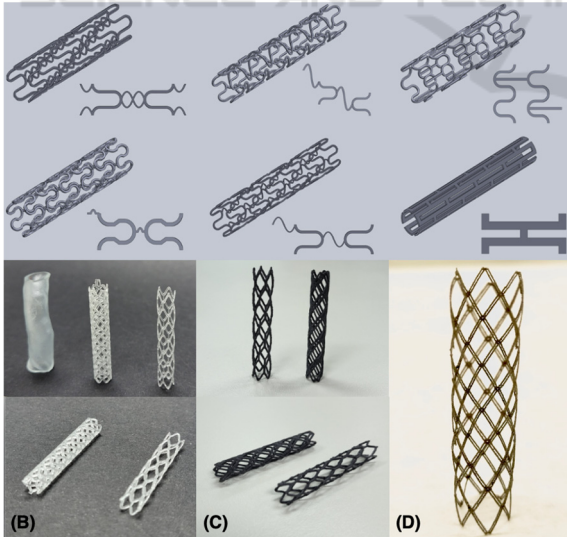


Figure 6: (A) Library of parameterized coronary stents. Prototypes manufactured by (B) stereolithography, (C) selective laser sintering and (D) melting.

The main objective of this methodology is to promote the creation of a parametrized coronary stent

library (Figure 6A). Therefore, physicians will have several options to select the one that best suits to the clinical and mechanical patient needs (Martínez Cendrero et al., 2022). Moreover, it will ensure a more personalized and simplified workflow by directly using the medical image and avoiding its segmentation.

4 CONCLUSIONS

The increasing demand of personalized biomedical solutions poses a major healthcare challenge. This proposal is a useful tool that aids custom stent modelling by adapting its cross-section to the internal artery cavity improving its fit and filling. Furthermore, this proof-of-concept avoids segmentation, as the arterial edge is extracted directly from the medical image, reducing the inherent errors of conventional workflow.

The integration of artificial intelligence and numerical methods in the web application has shown that elliptical sections are better adapted to the coronary artery and, from these fitted curves patient-specific stents can be designed. The web application transforms the designer's work into an inspector to ensure that the solution proposed by the application meets quality standards.

The main problems of personalized medicine are time-consumption and high economic cost. Therefore, the web application and parametric models, automatization tools, could be the solution related to the first issue, as they reduce the delivery times being the personalized prostheses competitive in emergency situations. Moreover, by using 3D printing, the price of personalized medical devices will be decreased significantly. Consequently, the combination of medical imaging, automatization tools and 3D printing could lead to new competitive, affordable, and accessible high-quality patient-specific implants.

5 FUTURE LINES

To balance the medical demand for personalized solutions, advances in computer vision, computational design and artificial intelligence will be critical to achieve full automatization of the implant's workflow (Figure 1). This will help designers produce a more aesthetic morphology and precise fit, as well as a higher level of customization and a comforting patient experience. This symbiosis of computational, mechanical, and biomedical

technologies will result in a new generation of customized prostheses that will improve clinical outcomes for millions of patients worldwide. This new methodology could be extrapolated to many clinical cases, such as aortic valves and hip prostheses (Solórzano Requejo et al., 2022).

ACKNOWLEDGEMENTS

The research presented has been supported by the project: "IMPLANTS-CM: impresión de metamateriales empleando aleaciones con memoria de forma y gradientes funcionales para una nueva generación de implantes inteligentes", funded by the "Convocatoria 2020 de ayudas para la realización de proyectos sinérgicos de I+D en nuevas y emergentes áreas científicas en la frontera de la ciencia y de naturaleza interdisciplinar" financed by Comunidad Autónoma de Madrid (ref. del proyecto: Y2020/BIO-6756).

The authors express their gratitude to Mar Cogollo, Adrián Martínez, Francisco Franco, Miguel Clavijo, Pedro Ortego, Javier Tuesta, Nicolás Kuroki, Leandro Velásquez and Daira Mena for inspiring and supporting us to conduct research that benefits society.

REFERENCES

- Černov, N. (2011). Circular and linear regression: Fitting circles and lines by least squares. CRC.
- Cockerill, I., See, C. W., Young, M. L., Wang, Y., & Zhu, D. (2021). Designing Better Cardiovascular Stent Materials: A Learning Curve. *Advanced Functional Materials*, 31(1), 2005361. <https://doi.org/10.1002/adfm.202005361>
- Díaz Lantada, A., Solórzano, W., Martínez Cendrero, A., Zapata Martínez, R., Ojeda, C., & Muñoz-Guijosa, J. M. (2022). Methods and Technologies for the Personalized Design of Open-Source Medical Devices. In A. Ahluwalia, C. De Maria, & A. Díaz Lantada (Eds.), *Engineering Open-Source Medical Devices: A Reliable Approach for Safe, Sustainable and Accessible Healthcare* (pp.191–218). Springer International Publishing. https://doi.org/10.1007/978-3-030-79363-0_9
- Fischler, M. A., & Bolles, R. C. (1981). Random sample consensus: A paradigm for model fitting with applications to image analysis and automated cartography. *Communications of the ACM*, 24(6), 381–395. <https://doi.org/10.1145/358669.358692>
- Fitzgibbon, A., Pilu, M., & Fisher, R. B. (1999). Direct least square fitting of ellipses. *IEEE Transactions on Pattern Analysis and Machine Intelligence*, 21(5), 476–480. <https://doi.org/10.1109/34.765658>
- Martínez Cendrero, A., Franco Martínez, F., Solórzano Requejo, W. G., & Díaz Lantada, A. (2022). Open-source library of tissue engineering scaffolds. *Materials & Design*, 223, 111154. <https://doi.org/10.1016/j.matdes.2022.111154>
- Moscol, I., Solórzano-Requejo, W., Ojeda, C., & Rodríguez, C. (2022). Personalized Hip Replacement: State of the Art and New Tools Proposals: Proceedings of the 15th International Joint Conference on Biomedical Engineering Systems and Technologies, 46–57. <https://doi.org/10.5220/0010823100003123>
- Pan, C., Han, Y., & Lu, J. (2021). Structural Design of Vascular Stents: A Review. *Micromachines*, 12(7), 770. <https://doi.org/10.3390/mi12070770>
- Paton, K. (1970). Conic sections in chromosome analysis. *Pattern Recognition*, 2(1), 39–51. [https://doi.org/10.1016/0031-3203\(70\)90040-3](https://doi.org/10.1016/0031-3203(70)90040-3)
- Paxton, N. C., Nightingale, R. C., & Woodruff, M. A. (2022). Capturing patient anatomy for designing and manufacturing personalized prostheses. *Current Opinion in Biotechnology*, 73, 282–289. <https://doi.org/10.1016/j.copbio.2021.09.004>
- Phantom Coronary Artery Models | NIH 3D Print Exchange. (n.d.). Retrieved 11 April 2022, from <https://3dprint.nih.gov/discover/3dpx-012589>
- Saçlı, H., Kara, İ., & Kirali, M. K. (2018). Focus on Coronary Atherosclerosis. In L. Gianturco (Ed.), *Atherosclerosis—Yesterday, Today and Tomorrow* (1st ed.). InTech. <https://doi.org/10.5772/intechopen.77301>
- Scafa Udriște, A., Niculescu, A.-G., Grumezescu, A. M., & Bădilă, E. (2021). Cardiovascular Stents: A Review of Past, Current, and Emerging Devices. *Materials*, 14(10), 2498. <https://doi.org/10.3390/ma14102498>
- Schillinger, M., Sabeti, S., Dick, P., Amighi, J., Mlekusch, W., Schlager, O., Loewe, C., Cejna, M., Lammer, J., & Minar, E. (2007). Sustained Benefit at 2 Years of Primary Femoropopliteal Stenting Compared With Balloon Angioplasty With Optional Stenting. *Circulation*, 115(21), 2745–2749. <https://doi.org/10.1161/CIRCULATIONAHA.107.688341>
- Solórzano Requejo, W., Martínez Cendrero, A., Aguilar, C., Zapata Martínez, R., Ojeda, C., & Díaz Lantada, A. (2022). Diseño de dispositivos médicos personalizados asistido por inteligencia artificial y métodos numéricos: Aplicación a prótesis articulares. Congreso Iberoamericano de Ingeniería Mecánica-CIBIM 2022. XV Congreso Iberoamericano de Ingeniería Mecánica. <https://doi.org/10.5944/bicim2022.094>
- Solórzano-Requejo, W., Ojeda, C., & Díaz Lantada, A. (2022). Innovative Design Methodology for Patient-Specific Short Femoral Stems. *Materials*, 15(2), Article 2. <https://doi.org/10.3390/ma15020442>
- Streamlit. (n.d.). Retrieved 3 October 2022, from <https://streamlit.io/>
- Tomberli, B., Mattesini, A., Baldereschi, G. I., & Di Mario, C. (2018). Breve historia de los stents coronarios. *Revista Española de Cardiología*, 71(5), 312–319. <https://doi.org/10.1016/j.recesp.2017.11.016>
- Trujillo-Pino, A., Krissian, K., Alemán-Flores, M., & Santana-Cedrés, D. (2013). Accurate subpixel edge

location based on partial area effect. *Image and Vision Computing*, 31(1), 72–90. <https://doi.org/10.1016/j.imavis.2012.10.005>

Wang, Q., Fang, G., Zhao, Y.-H., & Zhou, J. (2018). Improvement of Mechanical Performance of Bioresorbable Magnesium Alloy Coronary Artery Stents through Stent Pattern Redesign. *Applied Sciences*, 8(12), 2461. <https://doi.org/10.3390/app8122461>

